Macromolecules

ARTICLE

pubs.acs.org/Macromolecules

Viscosity Decrease and Reinforcement in Polymer−Silsesquioxane Composites

Klaus Nusser,* Gerald J. Schneider,* Wim Pyckhout-Hintzen, and Dieter Richter

Jülich Centre for Neutron Science and Institute for Complex Solids, Forschungszentrum Jülich GmbH, Jülich, Germany

Supporting Information

ABSTRACT: The rheological behavior of poly(ethylene-*alt*-propylene) (PEP), polydimethylsiloxane (PDMS) and polyisoprene (PI, two molecular weights: 70k and 200k) melts containing polyhedral oligomeric silsesquioxane (POSS) molecules was investigated by means of small angle scattering (SAXS and SANS) and oscillatory shear rheology. The dependence of the nanocomposite viscosity on the polymer−particle solubility and polymer molecular weight was studied. At high filler fractions all polymers exhibited hydrodynamic reinforcement of the plateau modulus quantified by a Guth Gold relation. Additionally, the PEP and PI70k systems showed a transition from liquid-like to solid-like rheological behavior. SAXS results enabled us to relate this behavior to the formation of a POSS network or POSS particle jamming, respectively. At low filler degrees, the zero shear viscosity of the nanocomposites was strongly dependent on the polymer solubility and entanglement number. We observed a viscosity decrease in the filled PDMS and PI200k samples, a constant viscosity in the PEP samples and regular reinforcement in the PI70k samples. These results are compared to the predictions of regular plasticization, and then quantitatively discussed in terms of the recently proposed model by Ganesan and Pyramitsyn, as well as the model by Wang and Hill. In particular the latter is shown to constitute a suitable means to quantify the results in terms of a layer of reduced polymer viscosity surrounding each nanoparticle.

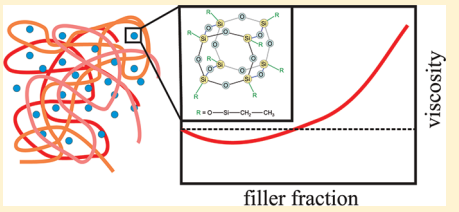

INTRODUCTION

The addition of solid particles into rubbery matrices has been technically used for more than a century now. The decisive advantage of the resulting polymer−filler nanocomposites lies in the drastic property changes induced by filler particles. An increase in use temperature, flammability reduction, better heat evolution, lower processing viscosity and reinforcement of the mechanical strength are only some of the macroscopic features which can be tuned by choosing an adequate amount and type of fillers.[1,2] In the context of this work we will focus on the exploration of the mechanisms responsible for the change of zero-shear viscosity and shear modulus of selected composites. A decade ago, this would have come down to the investigation of mechanical reinforcement of polymers by the addition of fillers.[2−6] Recently, however, the exact opposite was observed. The addition of very small nanoparticles lead to a significant reduction of the composite viscosity, which could not be explained by regular plasticization.[7] Being counterintuitive on first sight, this study triggered a flood of follow-up experiments, coming up with controversial observations and explanations.[8−16] Some of them indeed reported a viscosity decrease, lacking however any kind of quantitative interpretation. Still, the successful experiments exhibited some common preconditions that seem to be necessary for a viscosity decrease to occur. In particular, a filler particle size r_{part} smaller than the polymer radius of gyration R_g seems to be crucial. Moreover, filler−filler and filler−polymer interactions play an important role, which also manifests in the prerequisite of a good particle dispersion. Tuteja nicely summarized those common observations.[14]

With the need for suitably small particle diameters, polyhedral oligomeric silsesquioxanes (POSS) have come forward as a novel class of nano fillers (e.g., ref 17). Not only can they be regarded as the smallest possible and absolutely symmetric silica particles with core diameters as small as 1.5 nm (silica being one of the classically most investigated and employed fillers), but also do they allow grafting of a wide range of surface groups and thus variation of the filler−filler and filler−polymer interactions.[17−19] Unfortunately there is also a downside to this wide variety of different silsesquioxane molecules. Although a number of experimental studies on polymer-silsesquioxane nanocomposites have been published with interesting observations,[10,18−20] the used silsesquioxanes are never identical. To a certain extent this is, of course, inevitable in order to achieve good miscibility with the chosen polymer matrix. Furthermore, it is not damaging, as long as only the characterization of the properties of one special material system is intended. It is, however, very dissatisfactory from a physical point of view, when we predominantly aim to identify and clarify the mechanisms leading to viscosity decrease, reinforcement, or gelation in polymer−POSS composites.

For this reason, we chose to take a different approach. Instead of trying to detect one new polymer−POSS system optimized with respect to some property, we selected one type of POSS molecule with a simple, hydrophobic surface group (see Figure 1). This specific POSS molecule was chosen so that at least at low filler fractions good physical blending is expected for a variety of different polymers. As polymers poly(dimethylsiloxane) (PDMS), poly(ethylene-*alt*-propylene) (PEP) and polyisoprene (PI, two different

Received: July 12, 2011
Revised: August 29, 2011
Published: September 15, 2011

dx.doi.org/10.1021/ma201585v | *Macromolecules* 2011, 44, 7820–7830

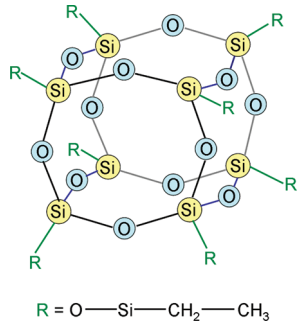

Figure 1. Scheme of a sx primary particle.

molecular weights) were chosen. The three polymer species differ only slightly from each other and from the POSS molecules concerning their Hansen solubility parameters (see Table 4). On the one hand, this guarantees the demanded good miscibility at low filler fractions. On the other hand, the magnitude of the solubility difference of the polymer species should still be high enough to clearly see its impact on the nanocomposite property change, when POSS particles are added. A characterization of the mechanichal properties of the four material systems was realized via oscillatory shear rheology, directly yielding the macroscopic viscosity and shear modulus as experimental observables. Additionally, small angle scattering was used to investigate the particle structure in the composites. This approach will enable us to experimentally classify the impact of polymer−filler solubility and polymer molecular weight.

EXPERIMENTAL SECTION

Materials. Four different model nanocomposite systems were used in this work, which differ concerning the polymer matrix. Poly(ethylene-*alt*-propylene) (═:PEP), poly(dimethylsiloxane) (═:PDMS) and two molecular weights of poly(isoprene) (═:PI) were employed. The nanoparticle species was identical in all samples. A scheme of the used silsesquioxanes with hydrophobic surface groups is given in Figure 1.

PI was synthesized by anionic polymerization of isoprene monomer, with *tert*-butyllithium as initiator and benzene as polymerization solvent. The obtained microstructure consists of 75% cis-1,4, 18% trans-1,4, and 7% 3,4 units. The weight-average molecular weights of the PI polymers were determined by low angle laser light scattering in heptane. The number-average molecular weight of PI was obtained from 1H-NMR measurements using the nine protons of the *tert*-butyl initiator group as internal reference. The polydispersities of all PIs were determined by size exclusion chromatography (SEC) in THF relative to polystyrene standards.

PEP was obtained by catalytic hydrogenation from a parent PI using a conventional Pd/$BaSO_4$ catalyst. Complete hydrogen saturation was verified by the disappearence of the vinyl protons in the ^{1}H NMR spectra. The average molecular weight of the obtained PEP was calculated from the measured parent PI weight by simply adding the mass of H_2 per repeat unit.

PDMS was supplied from the Max Planck Institute for Polymer Research in Mainz and characterized by means of SEC in octadecanol relative to polystyrene standards.

The detailed characteristics of all polymer species including molecular weight M_w, polydispersity M_w/M_n, radius of gyration R_g, entanglement molecular weight M_e and the radius of an entanglement segment R_e as well as the entanglement number $Z = M_w/M_e$ are summarized in Table 1.

The silsesquioxane nanofillers were obtained from Hybrid Plastics and will be referred to as "'Sx"' particles in this work. The chemical

Table 1. Properties of the Used Materials[a]

sample	M_w [kg/mol]	M_w/M_n	R_g (nm)	R_e (nm)	M_e (g/mol)	Z
sx	1.016	≈1	0.6	-	-	-
PEP	50	<1.02	9.1	3.7	1475	34
PDMS	190	<1.09	11.6	7.1	9613	20
PI70k	64.7	<1.02	8.6	5.5	5097	13
PI200k	254	<1.04	17.0	5.5	5097	50

[a] The values of the entanglement radius R_e and entanglement molecular weight M_e were taken from ref 21. R_g values are calculated except for PEP, where it was determined in an ancillary SANS experiment.

composition of the particles is $C_{16}H_{56}O_{20}Si_{16}$, the primary particle structure is schematically shown in Figure 1. According to supplier information, the particle diameter is $D_{sx} \approx 2$ nm, and the chosen surface rest group is hydrophobic. This results in good miscibility with the used apolar polymers. Furthermore, all nanocomposites in this study are governed by nonattractive interactions with exception of the ever-present van der Waals attraction.

The nanocomposite samples were obtained by means of solution mixing in toluene. After stirring for 48 h, the samples were first evaporated in air for 12 h and then dried in a vacuum oven for 48 h at T = 50 °C. The nomenclature in this work will denote each nanocomposite by its polymer matrix and the volume percentage of added sx particles. E.g., sample PI200k-1 consists of 99 vol % PI200k and 1 vol % sx.

Methods. *Small Angle Scattering (SANS and SAXS).* For the characterization of the silica filler structure in the nano composites, small angle X-ray scattering (SAXS) and small angle neutron scattering (SANS) images were recorded. The SAXS experiments were conducted on a NANOSTAR machine from Bruker AXS with a copper anode at 40 kV and 40 mA. The used wavelength was λ = 1.540 Å. The collimation was realized in pinhole geometry, the detector distance was 1.05 m. This results in an observed Q range 0.1 nm^{-1} < Q < 2 nm^{-1}. The SAXS measurements were conducted at ambient temperature with samples from the rheology after the rheological characterization.

Additionally a SANS experiment was conducted in order to resolve the single particle form factor of the Sx fillers. The sample contained 1 vol % Sx particles in deuterated toluene. The small-angle neutron scattering experiment was performed on the KWS-2 SANS instrument at the FRM II research reactor in Garching, München. The samples were measured at two different setups with sample-to-detector distances of L = 1.68m and 8m for 4.5 Å. For both setups a 8m collimation length was used. The wavelength spread was $\Delta\lambda/\lambda$ = 20%. With these setups the scattering vector Q covers a range of 8×10^{-3} Å$^{-1} \leq Q \leq 0.4$ Å^{-1}.

The raw data were corrected for the detector sensitivity, background noise and scattering from the empty cell, and calibrated in absolute units (cm^{-1}) by using a secondary standard (PMMA for SANS, FEP1400A bought from Dupont for SAXS) according to:

$$\left(\frac{d\Sigma}{d\Omega}(Q)\right)^{s} = \frac{(L^{s})^2 h^{sec} T^{sec} (d\Sigma/d\Omega)^{sec}}{(L^{sec})^2 h^{s} T^{s} T^{ec} \langle I^{sec} \rangle} ((I^{s}(Q) - I^{bg})(Q) - T^{s}(I^{ec}(Q) - I^{bg}))$$

Here pl, s, ec, and bg refer to the secondary standard, sample, empty cell, and background noise, respectively. T denotes the transmission, $I(Q)$ the scattered intensity, h the sample thickness, L the sample-to-detector distance, and $\langle I^{sec} \rangle$ the averaged measured intensity of the secondary standard. For SANS, after radial averaging, the calculated incoherent contribution of the Sx particles and measured scattering from solvent were subtracted in order to obtain the absolute normalized macroscopic differential cross section $(d\Sigma/d\Omega)(Q)$ of the Sx primary particle.

Rheological Characterization. All samples were characterized by means of dynamic mechanical spectroscopy. The measurements were performed on a strain-controlled Rheometric Sci. ARES system operated in the dynamic mode using 8 mm parallel plates. The samples were molded in a vacuum press for 60 min and then loaded. Sample loading took place at room temperature of 25 °C. The gap between the parallel plates was adjusted to about 1 mm initially and varied with temperature as to keep the normal force constant. The shear experiments were conducted with a shear amplitude of 0.5%, well within the linear viscoelastic regime of the samples. For data treatment, the software Orchestrator was used.

The measurements of PI70k and PEP samples were conducted in a temperature range from $T = -25$ to +25 °C and a frequency range from ω = 0.1 to 500 rad/s. The PI200k samples were measured in a temperature range from T = 25 to 61 °C. PDMS samples were only measured at 25 °C. The temperature stability was approximately 0.2 °C.

From the rheology measurements at different temperatures master curves were constructed using the 2-dimensional shifting option of the Rheometric Scientific Software (Orchestrator). The reference temperature T_0 was taken to be 25 °C for all curves and the horizontal shift factors a_T and vertical shift factors b_T were determined accordingly. The validity of the Williams−Landel−Ferry relationship[22] employed in the procedure

$$\log a_T = \log \frac{\tau(T)}{\tau(T_0)} = \frac{-C_1(T - T_0)}{C_2 + (T - T_0)} \tag{1}$$

is not straightforward in filled polymer systems and will be investigated in the Results section.

Independent of the applicability of TTS the relevant quantities η_0 and G_N^0 could in practically all cases be extracted from the data at 25 °C so that all conclusions are independent of the master curve construction.

THEORETICAL BACKGROUND

Small Angle Scattering (SANS and SAXS). In order to relate the structure of the sample to the intensity recorded by the scattering experiment the scattering cross section per unit volume $d\Sigma/d\Omega$ is defined by

$$\frac{d\Sigma}{d\Omega}(Q) = K\langle |A(Q)|^2 \rangle \tag{2}$$

K is a contrast factor, $A(Q)$ denotes the scattering amplitude, and the momentum transfer Q is defined by $Q = (4\pi)/(\lambda) \sin(\vartheta)$, where 2ϑ denotes the scattering angle.

When $QR_G \ll 1$, the so-called Guinier approximation

$$\frac{d\Sigma}{d\Omega} = I_0 \exp(-R_G{}^2Q^2/3) \tag{3}$$

is valid and is often used to determine R_G and $I_0 = \Phi(\Delta\rho)^2V_{part}$, where R_G the radius of gyration of the scattering object, V_{part} the particle volume, Φ the particle concentration and $(\Delta\rho)$ the scattering length density difference of particles and solvent.

The scattering curve of a structure with correlations dying out as $\exp(-r/\zeta)/r$ is a Lorentzian function,

$$\frac{d\Sigma}{d\Omega}(Q) = \frac{I_0}{1 + (Q\zeta)^m} + \text{const.} \tag{4}$$

ζ is the correlation length of the system and $m = 2$ for correlations dying out exponentially. If the loss of correlatioins is not really exponential due to screening effects and/or a mass fractal nature of the correlated scattering centers, the generalized form of eq 4 with $m \neq 2$ can be used to quantify the correlations in the sample.

Rheology. For the description of the viscoelastic properties of polymers there exist some elaborate models that interconnect macroscopic observations from rheological experiments with the molecular structure and dynamics of polymer melts. For the case of linear polymer melts a very good description was achieved by an implementation of the tube model described by Likhtman and McLeish.[23] Their molecular analysis of the complex shear modulus includes all elementary processes from short scale Rouse dynamics to reptation, accounting also for contour length fluctuations, constraint release and longitudinal modes. The governing material parameters in the model are the entanglement time τ_e, entanglement number Z, apparent disentanglement time τ_{df}(, which can be calculated from τ_e and Z), the plateau modulus G_e and a parameter c_ν, characterizing the influence of constraint release.

It cannot, however, be assumed a priori that a description of the composite materials' dynamics in terms of polymer dynamical processes is justified. Therefore, we chose a phenomenological spectral approach, based on the well-known BSW model in order to parametrize the effect of nanofiller addition into the polymer matrices.

The BSW model was for the first time empirically expressed by Baumgaertel, Schausberger, and Winter.[24] It is based on the fact that even a very complex relaxation process can always be described as a superposition of elementary relaxators with different characteristic relaxation times, in this case implemented as a continuous relaxation spectrum $H(\tau)$. In the dynamic mechanical experiments performed in this work, the complex dynamic shear modulus $G^*(\omega) = G'(\omega) + i \cdot G''(\omega)$ is measured and can be calculated calculated from the spectrum via

$$G'(\omega) = G_{elastic} + \int_{-\infty}^{+\infty} H(\tau)\omega^2\tau^2/(1 + \omega^2\tau^2)\, d(\ln \tau)$$
$$G''(\omega) = \int_{-\infty}^{+\infty} H(\tau)\omega\tau/(1 + \omega^2\tau^2)\, d(\ln \tau) \tag{5}$$

For un-cross-linked melts the permanent elastic contribution $G_{elastic}$ is 0. From the loss modulus G'' the zero-shear viscosity η_0 follows as

$$\eta_0 = \lim_{\omega \to 0}(G''/\omega) = \int_{-\infty}^{+\infty} H(\tau)\tau\, d(\ln \tau) \tag{6}$$

Note that the terminal behavior for $\omega \to 0$ generated by equation eq 5 is that characteristic of viscous flow with $G''(\omega) \propto \omega$ and $G'(\omega) \propto \omega^2$.

The ansatz orignially proposed by Winter for the spectrum reads

$$H(\tau) = H_e\tau^{n_e} + H_g\tau^{-n_g}, \quad \tau_0 < \tau < \tau_{max}$$
$$H(\tau) = 0, \quad \tau > \tau_{max} \tag{7}$$

$H_e = n_eG_N^0\tau_{max}{}^{-n_e}$ represents the entanglement regime, whereas $H_g = n_gG_N^0\tau_0{}^{-n_g}$ characterizes the glassy transition zone. More sophisticated spectra have been suggested in the literature, but the Winter spectrum proved to yield good results for our data. Although the spectrum cut off times τ_0 and τ_{max} lack a strict physical significance, they are connected with real physical quantities in the case of quite monodisperse linear polymers studied here. τ_0 compares to the relaxation time of an entanglement segment and is the shortest relaxation time considered in the model. The longest considered relaxation time τ_{max} on the

other hand corresponds approximately to the disentanglement time of a full chain.

The parameter G_N^0 is called the plateau modulus. In polymer nanocomposites a dependence of the plateau modulus $G_N^0(\Phi) = G_N^0(\Phi = 0) \times f(\Phi)$ on the filler degree Φ is usually observed.[25−27] For the expression $f(\Phi)$ a wide variety of choices exist in the literature and it is indeed the key to the understanding of the mechanisms in the composite material. The very general ansatz

$$f(\Phi) = 1 + [\eta]\Phi + a_2\Phi^2 + a_3\Phi^3 + \ldots \quad (8)$$

can be used to give a first parametrization of the results. For a classical system of a dilute solution of hard spheres in a solvent with no surface slip, Einstein[28] and later Smallwood[29] calculated the value of the intrinsic viscosity $[\eta] = 2.5$ by considering the flow disturbance and energy dissipation around a spherical particle in laminar flow of a Newtonian liquid. This solution is only a first order approximation of real systems and at higher filler fractions Φ interactions of two and more particles have to be included. The most successful, yet not analytically founded expansion was given by Guth and Gold,[30] who determined $a_2 = 14.1$ to be valid in a lot of systems. A theoretical calculation of the second-order coefficient was performed by Batchelor[31] and yielded $a_2 = 5.2$. Applying this value, however, often requires one to include a phenomenological third order coefficient a_3 in order to describe the data.

The examples mentioned so far all rely on the possibility to describe the system as a composition of perfect hard spherical filler particles in a Newtonian liquid. Einstein's hydrodynamic computations are only strictly valid when $r_{filler} > r_{solvmolecule}$.

A severe restriction to the applicability of the simple assumption of a hard sphere in a solvent is the fact that a polymer chain is not a small solvent molecule, but a macromolecule with an internal structure. Thus, a strong influence of the ratio $\gamma = R_{G,polymer}/r_{filler}$ with polymer radius of gyration R_G is expected in the domain of nano fillers, where $\gamma > 1$.

Moreover, real silica fillers feature a complex surface structure, often characterized by a large ratio of surface area to particle volume. Additionally enthalpic interactions of fillers and polymers, closely linked with the chemical structure of the materials, have to be considered. Consequently particle aggregation, chain adsorption on the particle surface as well as finite slip at the interface may occur in real systems. In many cases it has thus proven useful to employ an effective filler volume fraction Φ_{eff} rather than the real filler fraction Φ. In the simplest case a linear relation $\Phi_{eff} = \beta\Phi$ is assumed, where we will call β the effectiveness factor.

In dependence of these system variables a wide variety of values for $[\eta]$ have been observed,[7,12,25,32,33] most of which still lack a quantitative molecular interpretation.

At a certain critical filler loading Φ^* filler−polymer and/or filler−filler interactions may lead to the formation of a three-dimensional network in the sample. At the so-called gel point a connected network spanning the whole sample volume exists and the rheological behavior changes from melt-like to solid-like above a shortest network relaxation time τ^*. Viscous flow no longer appears in the terminal regime, but the zero-shear viscosity and the longest system relaxation time τ_{end} diverge. In the rheologically recorded curve of $G'(\omega)$ (or, respectively, $G''(\omega)$) the influence can easily be seen in the slopes at low ω deviating from the ω^2 (or ω^1 respectively) behavior.

To quantitatively include the possbility of gelation in the analysis, a gel relaxation contribution $H_{gel}(\tau)$ has to be added to the relaxation spectrum $H(\tau)$. For a critical gel, we define this contribution in accordance with the literature by a self-similar relaxation pattern[34]

$$H_{gel}(\tau) = S_{gel}/\Gamma(n)\tau^{-n} \quad (9)$$

for $\tau^* < \tau < \infty$. $\Gamma(n)$ is the gamma function, the amplitude S_{gel} represents the gel stiffness, and n is a relaxation exponent between 0 and 1. With this definition, the gel contribution to the storage and loss moduli can be written as[35]

$$G'_{critgel}(\omega) = \frac{G''_{critgel}(\omega)}{\tan(n\pi/2)} = S_{gel}\Gamma(1-n)\cos(n\pi/2)\omega^n \quad (10)$$

for $0 < \omega < 1/\tau^*$. Consequently, the ratio between storage and loss modulus of a critical gel is frequency independent:

$$\tan\delta_{critgel} = \frac{G''_{critgel}(\omega)}{G'_{critgel}(\omega)} = \tan\left(\frac{n\pi}{2}\right) \quad (11)$$

Note that for a polymer melt $d(\tan\delta)/d\omega < 0$, whereas for of a solid $d(\tan\delta)/d\omega > 0$.

In the case of a noncritical gel, this exact relation no longer holds and we define instead

$$G'_{gel}(\omega) = G'_{gel,0}\omega^n \qquad G''_{gel}(\omega) = G''_{gel,0}\omega^n \quad (12)$$

The exact value of the exponent n and the gel stiffnesses $G'_{gel,0}$ and $G''_{gel,0}$ have been found to be nonuniversal. They are, e.g., strongly dependent on the density and multiplicity of cross-links as well as on the strand length between cross-links.[36−41]

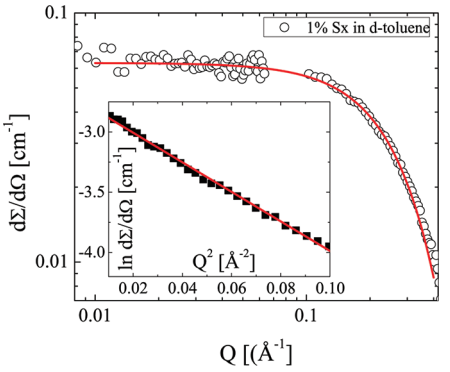

Figure 2. Form factor of an Sx primary particle as obtained from a SANS measurement of 1 vol % Sx in deuterated toluene. The inset shows the data in Guinier representation. The solid lines are the best Guinier fit.

RESULTS AND DISCUSSION

SANS and SAXS. Small angle neutron scattering (SANS) and small angle X-ray scattering (SAXS) were used to investigate the filler structure of the samples. Since the forward scattering contribution of an Sx primary particle in SAXS is too low for an accurate analysis on an absolute scale, we performed a SANS measurement for the characterization of the Sx primary particle. Figure 2 shows the scattering curve of 1 volume-% Sx in deuterated toluene. The Guinier regime of the primary particle is clearly visible and from a Guinier analysis a radius of gyration

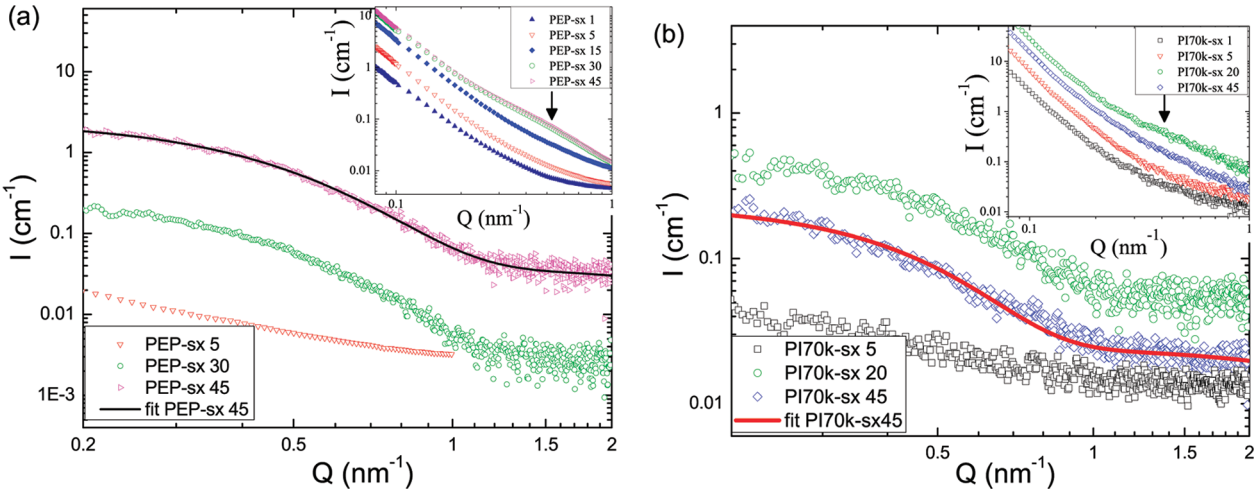

Figure 3. SAXS data for PEP (a) and PI70k (b) nanocomposite samples, where the forward scattering contribution was subtracted. The solid lines are best fits of the data with $\Phi = 45$ vol % according to eq 4. Insets: SAXS data including forward scattering contribution. The black arrows indicate the approximate position of the shoulder, which exists at high filler loadings.

Table 2. Parameters Used for Subracting the $10A\,Q^d$ Forward Scattering Contributions from the Data

	A	d
PI-1	−7.68	−4.05
PI-5	−7.37	−4.08
PI-20	−7.06	−4.11
PI-45	−6.61	−4.02
PEP-1	−4.04	−3.68
PEP-5	−3.63	−3.67
PEP-15	−3.15	−3.65
PEP-30	−3.05	−3.75
PEP-45	−3.07	−3.80

$r_g = (6.1 \pm 0.4)$Å can be extracted. From the forward scattering intensity I_0 the primary particle volume $V_{part} = (2100 \pm 200)$Å^3 was determined. This is consistent with the assumption that the Sx primary particles can be treated as compact spheres in good approximation: $V_{part} \approx 4\pi/3 \times (((5)/(3))^{1/2} r_g)^3$.

SAXS measurements were used to investigate the filler structure in dependence of filler fraction Φ. The insets of Figure 3 show the scattering curves of the PEP and PI70k nanocomposites. The curves with $\Phi = 45\%$ are shown on an absolute scale, normalized to the filler fraction. The scattering curves of PEP-20 and PEP-30 coincide at high Q with the PEP-45 curve after division by Φ, but are shifted by a constant factor in the plot for better visibility. The same is true for the curves of PI-20 and PI-45.

A quantitative analysis of the samples with small filler loadings is difficult due to the low signal-to-background ratio. It can be seen in Figure 3, however, that no indication of a scattering contribution apart from the polymer background is visible in the composites with filler degrees up to 15%. There is no dominating correlation length present in this case. This hints to a reasonable particle dispersion in the polymer matrix, which was earlier pointed out as a prerequisite for the observation of a viscosity decrease.

For all samples, a strong forward scattering contribution is visible, which may be attributed to scattering from voids and filler aggregates, i.e., a filler structure factor. A quantitative separation

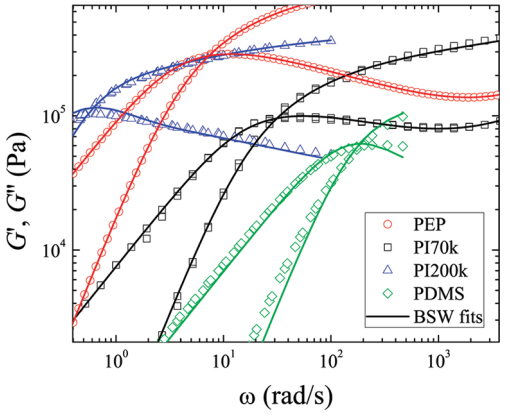

Figure 4. Rheology data for the unfilled polymer melts. Solid lines show fits with the BSW model according to eq 5.

of the contribution into a void and an aggregate part was not possible. The feature, which we want to point out and which is relevant for the analysis of the rheology data, is the shoulder, which appears at intermediate Q. The shoulder does not exist for $\Phi \leq 0.10$, whereas for $\Phi > 0.10$ it always appears at the same Q position. It clearly corresponds to a dominating correlation length, which can be estimated by use of eq 4. In order to make this more obvious, the $10A\,Q^d$ forward scattering contributions were subtracted from the data using the parameters summarized in Table 2. The remaining signal is depicted in Figure 3 in comparison with the best fits with eq 4. Because of the limited Q-range, reliable m's cannot be determined. Therefore, for the discussions below, m is not used. However for $1 < m < 3$ the correlation length ζ is hardly affected and quite invariant to changes of m. This way, $\zeta = 27.0 \pm 0.4$ Å is found in the PEP nanocomposites and $\zeta = 27.7 \pm 0.5$ Å in the PI70k samples. The existence of a correlation length ζ is attributed to the buildup of a gel-like Sx structure spanning the sample at high filler fractions $\Phi > \Phi^*$ with $10\% < \Phi^* < 20\%$.

Rheology. *Unfilled Polymers.* The measurements of samples with unfilled polymer melts constitute the basis for the following study of nanocomposites. Figure 4 shows the obtained rheology

dx.doi.org/10.1021/ma201585v |*Macromolecules* 2011, 44, 7820–7830

Table 3. Characterization of the Unfilled Polymer Melts[a]

sample	$G^0_{N,BSW}$	$\tau_{max}(s)$	$\tau_0(s)$	n_e	n_g	$G_{N,Fetters}$
PEP	1.15E6	0.31	1E−6	0.28	0.65	1.2E6
PDMS	0.16E6	0.01	-	-	-	0.2E6
PI70k	4.1E5	0.08	3.9E−6	0.27	0.60	0.4E6
PI200k	4.2E5	5.3	3.9E−6	0.24	0.60	0.4E6

[a] Values for $G_{N,Fetters}$ were taken from the literature.[21]

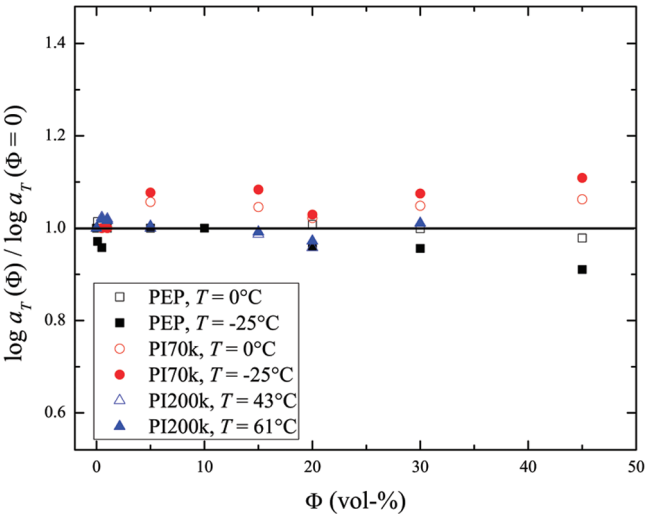

Figure 5. $\log a_T(\Phi)/\log a_T(\Phi = 0)$ for all nanocomposites and all shift temperatures.

data sets of the four different polymer matrices together with the best fit according to eq 5. In Table 3, a summary of the resulting parameters is given. For PDMS no reasonable values for n_e, n_g, and τ_0 were found, because the impact of these parameters is only visible at higher frequencies ω out of the experimental window. The obtained plateau moduli $G^0_{N,BSW}$ are compared with literature values $G_{N,Fetters}$[21] and indeed show satisfactory agreement.

Time−Temperature Superposition. From the rheology measurements at different temperatures master curves were constructed using the WLF equation (eq 1). In filled polymer nanocomposites, this procedure is not a priori justified.

It turned out, however, that the shifting procedure could be performed with the same WLF parameters C_1 and C_2 for all samples with the same polymer matrix, which underlines the applicability of the WLF equation in the investigated temperature range. This is best illustrated in Figure 5, where the ratio $\log a_T(\Phi)/\log a_T(\Phi = 0)$ is plotted for all samples in dependence of Φ. The validity of the WLF equation implies that the relaxation processes are still rheologically simple in the polymer sx nanocomposites. Moreover it can be deduced that in the ω-range where TTS resulted in a curve overlap, the temperature dependent relaxation probed was that of the polymer segments. The vertical shift factors b_T were in the range from 0.8 to 1.2 as expected from density and temperature factors.

Low Filler Fractions. The SAXS investigation already revealed the formation of a correlated sx structure, herein referred to as an Sx gel, above a critical filler volume fraction $\Phi^* > 10\%$. Hence it makes sense to discuss the behavior of the samples for $\Phi < \Phi^*$ and $\Phi > \Phi^*$ separately.

As can be seen in Figure 6 the relation $f = G^*(\omega,\Phi)/G^*(\omega,\Phi = 0)$ is fullfilled in good approximation for all polymer matrices by a

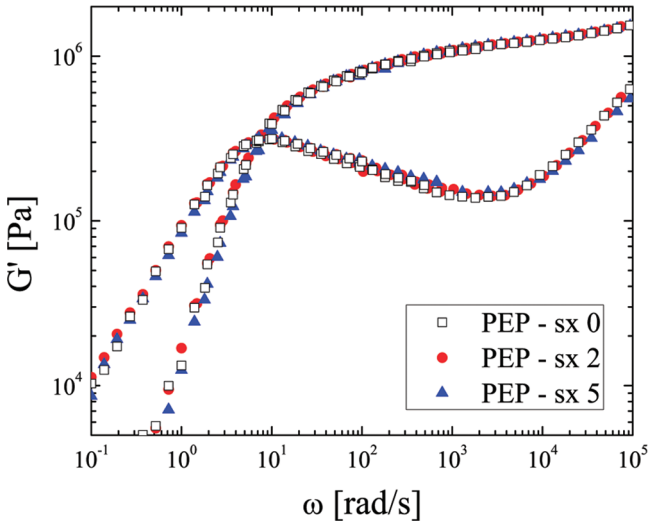

Figure 6. Storage modulus of various PEP samples with low filler fractions $\Phi < 10\%$ vs shear frequency ω. Exemplary for all systems, no change of the relaxation spectrum is visible for low filler fractions.

solely Φ-dependent multiplier $f(\Phi)$. No dependence $f(\omega)$ is observed, meaning that the overall shape of the curve is unaltered (the values of f for each system can be found in Figure 7 and Figure 8). The underlying spectrum $H(\tau)$ of relaxation times is thus only changed by a constant amplitude factor. This also means that all conclusions in the low-Φ-regime come down to the Φ-dependent analysis of the plateau modulus G^0_N or equivalently the zero-shear viscosity η_0. Note that the definition of η_0 includes an extrapolation of $G''(\omega)$ toward $\omega = 0$. This extrapolation is well-defined only in the low-Φ regime, where all samples actually enter a terminal regime characterized by mere viscous flow. Figure 7 shows the behavior of the zero shear viscosity for the 4 different polymer matrices under variation of the filler degree. The solid line is the best fit according to the Guth−Gold relation, i.e. according to eq. Equation 8 up to second order in Φ with $[\eta] = 2.5$, $a_2 = 14.1$, where additionally Φ was replaced by $\Phi_{eff} = \beta\Phi$ with an effectiveness factor β. This description will be shown to hold at higher filler loadings later (compare Figure 8 and Table 5).

For the understanding of the data, it will be helpful to introduce an appropriate measure for the mutual solubility of polymer species and sx particles. For this purpose we turn to the Hansen solubility S, which is supposed to be a reasonable approximation for the case of apolar materials. S is defined as the square root of the cohesive energy density $S = ((\Delta H_v - RT)/(V_m))^{1/2}$.[42] The solubilities for our materials are summarized in Table 4. Where existing, experimental values are given and compared to a calculation. For the calculation of S_{calc} the method presented by Hoftyzer and van Krevelen (see ref 42, pp 213ff.) was used, where also dispersive and polar contributions to S were accounted for. Since no tabulated values for the contribution of Si were available for this method, the experimental solubility value for PDMS[43] was used to estimate the Si group contribution in the appropriate configuration with four single bonds. This estimate was then used for the calculation of the Sx solubility, where the Si atoms also prevail in the same 4-single-bonded structure. The relevant quantity for mutual solubility is then the difference $\Delta S = |S_{Sx} - S_{polymer}|$. Small values indicate good solubility.

With this knowledge, we will turn to the inspection of the Φ dependent behavior of the zero shear viscosity. Obviously at low

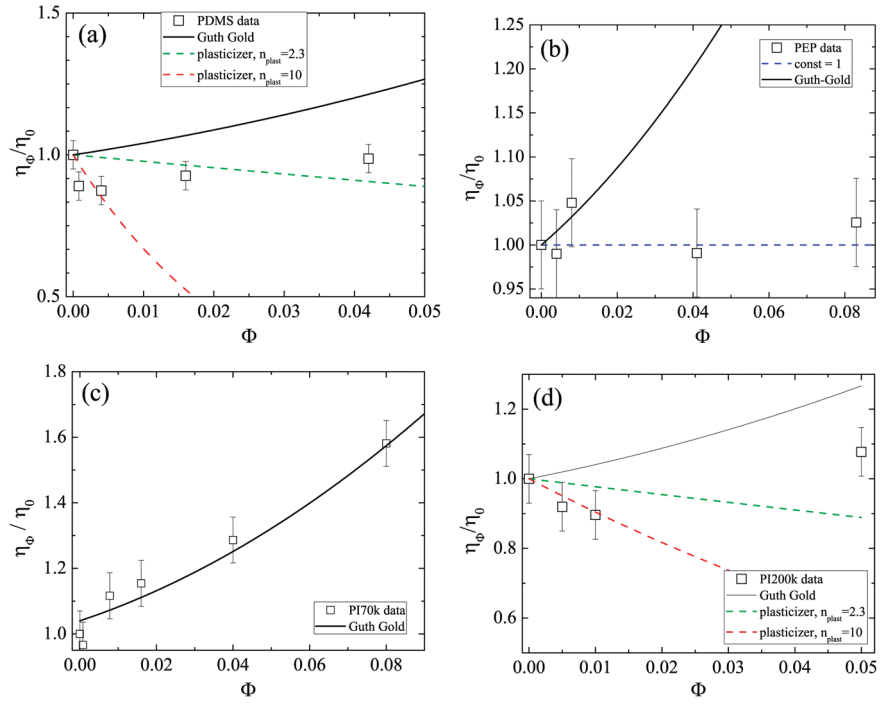

Figure 7. Zero shear viscosity ratio $\eta_0(\Phi)/\eta_0(\Phi = 0)$ of PDMS (a), PEP (b), PI70k (c), and PI200k (d) with Sx for low filler fractions Φ. The various lines represent model descriptions, explained in the text. Note that for low filler degrees $\eta_0(\Phi)/\eta_0(\Phi = 0) = G_{N,0}(\Phi)/G_{N,0}(\Phi = 0)$.

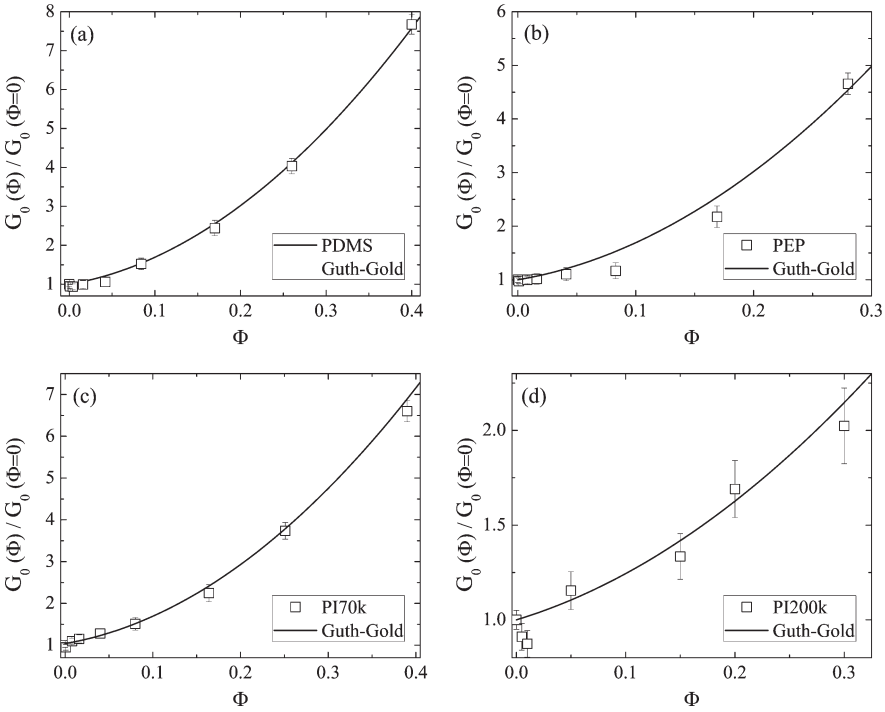

Figure 8. Storage modulus G_N^0 vs filler fraction Φ for all samples. The solid lines are fits with the Guth−Gold function and an effectiveness factor β.

filler degrees only PI70k samples follow the Guth-Gold relation. Note that polyisoprene is the material with the least solubility for the Sx particles with $\Delta S = 1.3$ J/cm^3.

In the PEP nanocomposites the zero shear viscosity remains constant in good approximation in the whole range up to 10 vol % Sx loading, which is well below the classical hydrodynamic prediction from Einstein. $\Delta S_{PEP} = 1$ indicates a slightly better Sx solubility in PEP than in PI, but worse solubility than in PDMS, where $\Delta S_{PDMS} = 0.3$.

Indeed, the PDMS composites reveal a significant decrease of the plateau modulus at very small Φ and only at 10% filler loading the Guth−Gold line is reached.

dx.doi.org/10.1021/ma201585v |*Macromolecules* 2011, 44, 7820–7830

Table 4. Solubility Parameters (in Units of $MPa^{0.5}$) and Plasticization Exponents

sample	solubility S_{exp}	S_{calc}	n_{plast}
Sx	-	15.0	-
PEP	15.8[44]	16.0	-
PDMS	15.3[43]	15.3	10
PI70k	16.3[44]	16.3	-
PI200k	16.3[44]	16.3	10

In the PI200k composites, despite the bad solubility of polyisoprene for the Sx particles, a similar modulus decrease is observed at low filler degrees. Note that PI200k is the matrix with the highest entanglement number Z, indicating a dependency on molecular weight (cf., e.g., refs 32 and 45).

For reasons described in the Background section the failure of the classical hydrodynamic description according to Einstein is not at all suprising. All of the used polymers have a ratio $\gamma = R_g/r_{part} > 1$ (cf. Table 1), which sets us in need to consider different solutions of the problem.

First, a comparison with the regular plasticization of polymer matrices by the addition of small molecules will be performed. One of the demanded prerequisites for a system to be plasticized is indeed the condition that $\gamma > 1$. The failure of a classical plasticization ansatz is visualized in Figure 7, where the formula $G(\Phi)/G_0 = (1 - \Phi)^{n_{plast}}$ characteristic for plasticization[46] is shown as a dashed red line with $n_{plast} = 10$. Usual experimental values for the exponent n_{plast} are in the range $2.0 < n_{plast} < 2.3$.[27,32] Obviously the description is not appropriate.

Instead, a solution for the hydrodynamic problem in the range $l_{mono} < r_{filler} < R_{e,polymer}$ needs to be found, which also considers nonzero slip at the particle surface. Quite recently interesting approaches in that regime were suggested by Ganesan and Pyramitsyn[47] and by Wang and Hill,[48] which may contribute to a more quantitative understanding in the future.

In the following section, we will very briefly mention the basic ideas of these two approaches and try to apply them to our experimental data. In the publication we will only focus on the decisive results and conclusions of this attempt, the details of the procedure are given as Supporting Information.

The approach suggested by Ganesan and Pyramitsin[47] includes an explicit solution of the hydrodynamic Navier−Stokes equations of the system. The filler particles are considered as spherical, and the influence of the polymer−filler size ratio as well as finite slip at the filler surface is included. The two decisive parameters of the theory are consequently the size ratio $\gamma = R_g/r_{filler}$ and the dimensionless slip length $\lambda_{gan} \geq 0$, where $\lambda_{gan} = 0$ corresponds to no slip. Dependent on the actual values of λ_{gan} and γ, a viscosity change $\Delta\eta$ is predicted according to

$$\frac{\Delta\eta}{\eta_0(\Phi = 0)} = \frac{3 - 96\lambda_{gan}\gamma^2}{2(1 + 5\lambda_{gan} + 48\lambda_{gan}\gamma^2)}\,\Phi \qquad (13)$$

Note that the calculation in ref 47 is performed for the case of unentangled polymers, but the authors suggest the extension to the entangled case by a simple estimate (see Supporting Information for details); in particular, the quantity relevant for the size ratio γ has to be identified with the polymer entanglement distance instead of the radius of gyration, i.e. we redefine $\gamma = R_e/r_{filler}$. Now γ can easily be calculated from the known material properties, leaving λ_{gan} as the only free parameter for the description of our experimental data of PI200k and PDMS at low filler fractions. It turns out, however, that it is impossible to find a slip value λ_{gan} so that the calculations fit the experimental data. The predicted viscosity reduction by eq 13 is always much smaller than the experimentally observed one. We conclude that a quantitative description within the framework of the Ganesan theory is not yet possible for the case of entangled polymer melts.

Table 5. Effectiveness Factors for Guth−Gold Interpretation of High Filled Samples

sample	β
PEP	1.50
PDMS	1.59
PI70k	1.44
PI200k	0.70

Next, we turn to a different ansatz suggested by Wang and Hill.[48] Their explicit goal was to describe the results about viscosity reduction in polymer nanoparticle composites reported by Tuteja and Mackay[7,9] using a continuum model. To achieve this, Wang and Hill assume the presence of a layer of polymer at the particle−polymer interface (thickness δ), which differs from the bulk regarding viscosity and/or density. The existence of such a layer with changed density/viscosity has also been found in various simulations (e.g., refs 49−53). Moreover, in the present case, a plausibility argument can be brought forward in order to justify this assumption. A nano particle of the size $l_{mono} < r_{filler} < R_{e,polymer}$ cannot diffuse freely in a polymer melt, but is subject to polymer Rouse motion. The reason for this is that any particle movement is always reliant on the rearrangement of the surrounding polymer segments, which follow Rouse motion on the length scale of the nano particle dimensions. As a consequence, Wang and Hill postulate a layer of thickness δ on the order of the entanglement distance R_e surrounding each nano particle, where the viscosity in the layer (η_{in}) is equivalent with the formal Rouse viscosity, $\eta_{in} = \eta_{Rouse}$. In this case η_{Rouse} is the viscosity calculated by the Rouse model, which a polymer chain of the melt would adopt, if it was subject to Rouse dynamics instead of reptation dynamics. This quantity is obviously significantly smaller than the bulk viscosity (η_{out}), which is given by the regular reptation model, $\eta_{out} = \eta_{rep}$.

Moreover they account for finite slip at the particle surface by means of a reciprocal slipping length k_{Wang}. The conventional no-slip boundary conditions are reflected by $k \rightarrow \infty$, whereas $k = 0$ corresponds to polymers slipping without resistance along the nanoparticle surface. With these definitions they solve the Stokes equation focusing on the regime of shear rates $d\gamma/dt \approx 10^{-3}s^{-1}$, $\eta \approx 10^5$, $r_{part} \approx 10$ nm, and $R_G \approx 10$ nm, which is in good agreement with the experimental parameters in our experiments. As a result, for each filler fraction Φ the viscosity change $[\eta]$ is found as a function of δ, η_{in}/η_{bulk}, and k_{Wang}.

Now η_{in}/η_{bulk} can be calculated directly from the polymer properties and is found to be $\ll 1$ in all our systems. For this case, Wang and Hill showed that the choice of k_{Wang} has only very little influence on the results and can be set to $k_{Wang} = 0$. The only remaining free parameter is thus the thickness of the surface layer δ, which can then be easily calculated for each sample from the experimental observations in our rheology measurements.

That way, one finds that the constant viscosity of the PEP samples at low filler fractions corresponds to a layer thickness $\delta_{PEP} = 0.83$ Å, which is universal for the low filler fractions Φ. For the PDMS samples the layer thickness strongly depends on the

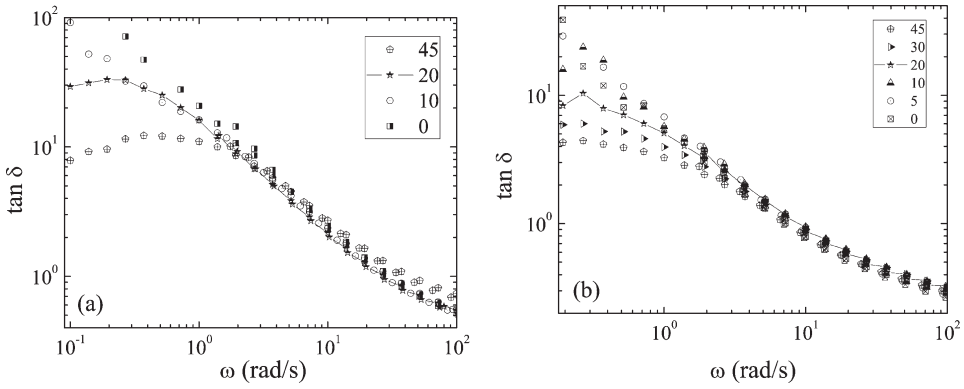

Figure 9. tan(δ) for PEP (a) and PI (b) samples. Obviously the gel point is in both cases between 10 and 20%.

actual filler degree and reads for the 3 smallest silica fractions $\delta_{PDMS}(0.1\%) = 26.6$ Å, $\delta_{PDMS}(0.5\%) = 13.3$ Å, and $\delta_{PDMS}(2\%) = 3.2$ Å. We want to note that PFG experiments on PDMS silicate composites, with a particle size of 3.5 Å give similar values.[54] The results for the PI200 K samples are similarly $\delta_{PI200k}(0.5\%) = 8.9$ Å and $\delta_{PI200k}(1\%) = 6.7$ Å. These estimated thicknesses of the layer with Rouse viscosity are in all cases significantly smaller than the corresponding tube diameter of the material and may thus be taken as the most realistic interpretation of the occurring processes available so far. Note that the decreasing layer thicknesses do not necessarily mean that the actual layer thickness around each particle decreases. The values given are mean values, so it is rather likely that with increasing volume fraction Φ there is an amount of particles with identical layer thickness, but also an amount of particles, which aggregate and do not contribute to the viscosity decrease anymore. The latter decrease the value of the mean layer thickness. No values for the PI70k system were calculated, because no viscosity decrease was observed there. The details of the calculation are given in the Supporting Information.

Of course, the Wang/Hill model is only a continuum approximation for the very complex problem of entangled polymer dynamics in the presence of nanoparticles. Nevertheless, the success of the description may indicate that there is some truth in their assumptions. In particular, their main claim, i.e., the existence of a layer with reduced viscosity near the particle surface seems to be very plausible and the layer thickness can serve as a reasonable means of quantification.

High Filler Fractions. At high filler loadings $\Phi > \Phi^*$ the rheological behavior of the samples can be understood largely in the classical picture of hydrodynamic reinforcement, as far as the plateau modulus is concerned. The ratio $G^0(\Phi)/G^0(\Phi = 0)$ is shown for the four sample systems in Figure 8. The dependence of the plateau modulus $G_N^0(\Phi)$ is well-described by the often used Guth−Gold relation[30] with an effectiveness factor β (see Background section), as shown by the solid lines in Figure 8). In the PI200k samples, an effectiveness factor $\beta = 0.7$ was observed. This indicates that chain length effects may lead to slippage at the particle surface, lowering the effective hydrodynamic reinforcement. The postulated existence of a molecular weight dependence, which was also implied as an explanation of the different observations for PI70k and PI200k at low filler degrees, is thus confirmed by this high-Φ behavior.

In PDMS, PEP and PI70k we get $\beta \approx 1.5$. This equivalence of high-Φ-behavior corroborates the comparability of the results at low Φ for these three composite materials.

Table 6. Relaxation Strengths of the Second Relaxation Process in High Filled PEP and PI70k Samples

sample	$G'_{gel,0}$ [kPA]	$G''_{gel,0}$ [kPA]	n_{sec}
PEP-20	10.8	56.6	0.88 ± 0.2
PEP-30	53	104	0.87 ± 0.3
PEP-45	134	219	0.87 ± 0.3
PI70k-20	0.26	0.79	0.8 ± 0.2
PI70k-30	1.1	5	0.8 ± 0.3
PI70k-45	3.3	15	0.55 ± 0.3

For low filler fractions the consideration of the plateau modulus $G_N^0(\Phi)$ in dependence of Φ or equally the zero shear viscosity $\eta_0(\Phi)$, which was linearly related to G_N^0 in all investigated systems, contained all changes of the rheological behavior of the samples. The shape of the relaxation spectra remained unchanged. At filler loadings $\Phi \geq 20\%$, this is not true anymore in the PEP and PI70k samples. The regime of viscous flow in the terminal regime disappears at high filler fractions Φ. Figure 10 illustrates, how the slopes in $G'(\omega)$ become smaller with increasing filler degree at $\omega < 3$ rad/s. They significantly deviate from the ω^2-behavior observed at low filler fractions. No such deviations were observed in the PDMS and PI200k samples.

The loss of viscous flow points to interparticle or particle−matrix interactions leading to a transition from melt-like to solid-like behavior (e.g., refs 18, 19, and 27). Remembering that $d(\tan\delta)/d\omega < 0$ for polymer melts/liquids and $d(\tan\delta)/d\omega > 0$ for solid bodies, we are provided with a means to identify the experimental gel point, i.e. the filler volume fraction Φ^*, where a critical gel is formed. The tan δ for relevant samples of the PEP and PI70k system is plotted in Figure 9. A change in the slope of the curves at low ω from melt-like to solid-like is clearly visible with increasing filler fraction. Obviously for PEP, the gel point is quite close to $\Phi = 20\%$. In the PI70k system $10\% < \Phi^* < 20\%$ is observed.

For a quantitative description of the data we now include a gel relaxation term $G^*_{gel}(\omega)$ as described in the Theoretical section with gel relaxation strengths $G'_{gel,0}$ and $G''_{gel,0}$. Table 6 gives the best parameters obtained from fits with the gel expanded BSW spectrum. The corresponding curves are depicted in Figure 10. The values for the PEP-20 and PI-20 samples are in good agreement with the assumption of a critical gel with gel strength $S_{PEP} = 7.33$ kPa and $S_{PI} = 0.18$ kPa. The higher filled samples do not obey the critical gel relation any more, but a monotonous increase of the gel relaxation strengths with increasing filler fraction is observed.

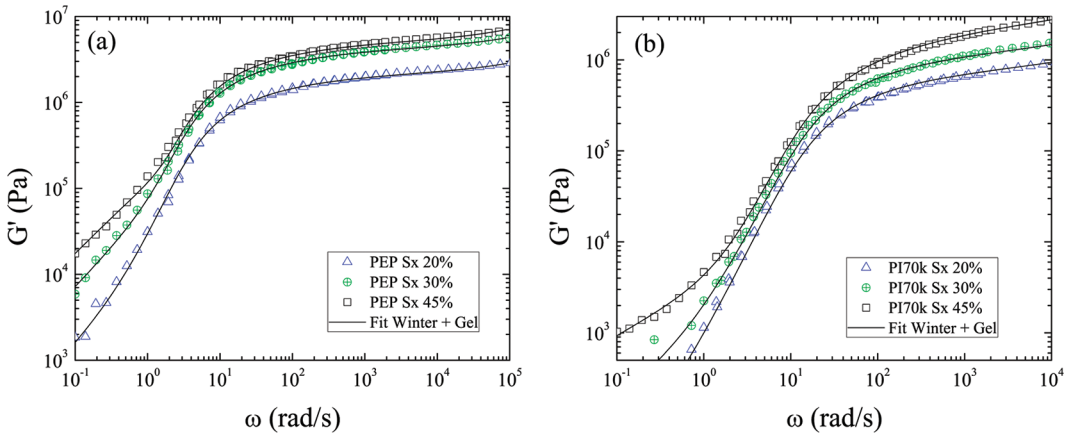

Figure 10. Storage moduli of high filled PEP (a) and PI70k (b) samples, which exhibit an additional relaxation process at low frequencies ω, distinguished by the loss of viscous ω^2-behavior. The solid lines are fits with the Winter spectrum after the addition of a gel relaxation term.

The magnitudes of S_{PEP} and S_{PI} of the two systems reveal strikingly different absolute values, with S_{PEP} being approximately an order of magnitude higher than S_{PI} at the same Sx volume fraction. This is mainly due to the different viscosities of the parent polymer matrices $\eta_{0,PEP} \approx 12\eta_{0,PI70}$, which constitute the medium for the interpenetrating sx aggregate structure. An analogueuous behavior has been observed in the literature. Fu et al. witness the formation of a particle−particle network in a system of highly filled PEP with POSS particles similar to ours.[18] Similarly, Zhou et al. find a particle gel in polypropylene-POSS nano composites.[19]

CONCLUSION

Melts of poly(ethylene-*alt*-propylene) (PEP), poly(dimethylsiloxane) (PDMS), and polyisoprene with two different molecular weights (PI70k, PI200k) were filled with polyhedral oligomeric silsesquioxane nanoparticles. It was shown that the filler particles cause hydrodynamic reinforcement in all cases at sufficiently high filler fractions Φ, where the reinforcement factor was quantitatively modeled with the Guth Gold relation and an effective volume fraction $\beta \approx 1.5$ (except for the PI200k samples, where $\beta = 0.7$). In the PEP and PI70k system, a transition from liquid-like to solid-like rheological behavior was observed with increasing filler fraction. In agreement with this, the existence of a POSS gel/aggregate structure with correlation length $\zeta \approx 27$ Å was observed by SAXS.

The relaxation strengths of the critical gels are an order of magnitude different for PEP (S = 10.8 kPa) and PI70k (S = 0.26 kPa). This was attributed to the different viscosities of PEP and PI70k.

At low filler degrees the four sample systems exhibited strong differences. Reinforcement was observed in the PI70k samples, neither reinforcement nor viscosity decrease in the PEP samples, and a viscosity decrease in the PI200k and PDMS samples. Special attention was given to the analysis of the viscosity decrease in PI200k and PDMS. In particular the notion of plasticization was rejected because of an unrealistically high plasticization exponent $n_{plast} = 10$.

The qualitatively different behavior of the model systems at low Φ emphasizes the importance of the influence of polymer−particle solubility ΔS, the relative polymer−particle length scales R_g/r_{part} as well as entanglement number Z. In particular the influence of mutual solubility has not been paid enough attention to in current model descriptions. It has already been emphasized in the literature[14] that a necessary prerequisite for the occurrence of a viscosity decrease is a good dispersion of the nanoparticles. In this context, however, mainly the importance of the sample preparation method was stressed. The solubility was only mentioned insofar that the polymer and particle be soluble enough to prevent clustering. Even more, no variation of the solubility was studied, but only the enthalpically identical components "'linear polystyrene chains"' and "'highly crosslinked polystyrene nanoparticles"' were used, which constitutes the case of optimal solubility. In our work, we have confirmed this notion by concluding that in all sample systems regular reinforcement is observed at high filler fractions Φ, when particle clusters exist.

Our results do not stop here, however, but go one step beyond this by studying systems with slightly different solubilities. Our experiments have shown that the absence of clusters and the correct polymer−particle size ratio are not enough. Instead the solubility itself plays a major role for the nanoparticle impact on the composite viscosity. Future considerations will have to include this issue, e.g. in terms of a solubility dependent slip length (see, e.g., ref 47 for the idea of a theoretical approach) or a layer of changed friction or density near the interface between polymers and particles (see, e.g., ref 48). An interesting implementation of these ideas in the shape of a continuum model was suggested by Wang and Hill[48] and applied to the experimental data of this work. The resulting estimations for the thickness of a layer δ of changed viscosity surrounding each nanoparticle are in a very reasonable order of magnitude, backing up the basic idea.

ASSOCIATED CONTENT

Supporting Information. Results of a comparison of the experimental data with the theoretical approach by Ganesan and that by Wang and Hill. This material is available free of charge via the Internet at http://pubs.acs.org.

AUTHOR INFORMATION

Corresponding Author

*E-mail: (K.N.) k.nusser@fz-juelich.de; (G.J.S.) g.j.schneider@fz-juelich.de.

■ ACKNOWLEDGMENT

The authors thank L. Willner for the used polymers and A. Radulescu for assistance at the JCNS SANS instrument KWS-2. K.N. acknowledges the financial support of the Evonik Stiftung.

■ REFERENCES

(1) Joshi, M. B.; Butola, S. *J. Macromol. Sci., Part C: Polym. Rev.* **2004**, *44*, 389.
(2) Kraus, G. *Reinforcement of Elastomers*; John Wiley & Sons: New York, 1965.
(3) Donnet, J.-B.; Voet, A. *Carbon Black: Physics, Chemistry and Elastomer Reinforcement*; Marcel Dekker, Inc.: New York, 1976.
(4) Medalia, A. I. *Rubber Chem. Technol.* **1978**, *51*, 437.
(5) Wolff, S.; Wang, M. J.Carbon Black Reinforcement of Elastomers. In *Carbon Black: Science and Technology*, 2nd ed.; Donnet, J. B., Bansal, R. C., Wang, M. J., Eds.; Marcel Dekker: New York, 1993; Chapter 9.
(6) Wang, M.-J. *Rubber Chem. Technol.* **1998**, *71*, 520.
(7) Mackay, M. E.; Dao, T. T.; Tuteja, A.; Ho, D. L.; B., v.; Kim, H.-C.; Hawker, C. J. *Nat. Mater.* **2002**, *2*, 762–766.
(8) Mackay, M. E.; Tuteja, A.; Duxbury, P. M.; Hawker, C. J.; Van Horn, B.; Guan, Z.; Chen, G.; Krishnan, R. S. *Science* **2006**, *311*, 1740–1743.
(9) Tuteja, A.; Mackay, M. E.; Hawker, C. J.; van Horn, B. *Macromolecules* **2005**, *38*, 8000–8011.
(10) Hao, N.; Böhning, H.; Goering, H.; Schönhals, A. *Macromolecules* **2007**, *40*, 2955.
(11) Tuteja, A.; Duxbury, P. M.; Mackay, M. E. *Phys. Rev. Lett.* **2008**, *100*, 077801−1–077801−4.
(12) Jain, S.; Goossens, J. G. P.; Peters, G. W. M.; van Duin, M.; Lemstra, P. J. *Soft Matter* **2008**, *4*, 1848–1854.
(13) Tuteja, A.; Mackay, M. E.; Narayanan, S.; Asokan, S.; Wong, M. S. *Nano Lett.* **2007**, *7*, 1276–1281.
(14) Tuteja, A.; Duxbury, P. M.; Mackay, M. E. *Macromolecules* **2007**, *40*, 9427–9434.
(15) Jain, S.; Goossens, J. G. P. M. v. *Macromol. Symp.* **2006**, *233*, 225–234.
(16) Jain, S.; Goossens, H.; van Duin, M.; Lemstra, P. *Polymer* **2005**, *46*, 8805–8818.
(17) König, H. J. *Silsesquioxane mit oligomeren Käfigstrukturen*; Dissertation, Universität Paderborn: Paderborn, Germnay, 2002.
(18) Fu, M. Y. ; Gelfer, B. X.; Hsiao, B. S.; Phillips, S.; Viers, B.; Blanski, R.; Ruth, P. *Polymer* **2003**, *44*, 1499–1506.
(19) Zhou, Z.; Zhang, Y.; Zhang, Y.; Yin, N. *J. Polym. Sci., Part B* **2008**, *46*, 526–533.
(20) Hao, N.; Böhning, M.; Schönhals, A. *Macromolecules* **2007**, *40*, 9672–9679.
(21) Fetters, L. J.; Lohse, D. J.; Richter, D.; Witten, T. A.; Zirkel, A. *Macromolecules* **1994**, *27*, 4639–4647.
(22) Williams, M. L.; Landel, R. F.; Ferry, J. D. *J. Am. Chem. Soc.* **1955**, *77*, 3701.
(23) Likhtman, A. E.; McLeish, T. C. B. *Macromolecules* **2002**, *35*, 6332–6343.
(24) Baumgärtel, M.; Schausberger, A.; Winter, H. H. *Rheol. Acta* **1990**, *29*, 400–408.
(25) Eggers, H.; Schuemmer, P. *Rubber Chem. Technol.* **1996**, *69*, 253–265.
(26) Heinrich, G.; Klüppel, M.; Vilgis, T. A. *Curr. Opin. Solid State Mater. Sci.* **2002**, *6*, 195–203.
(27) Kopesky, E. T.; Haddad, T. S.; McKinley, G. H.; Cohen, R. E. *Polymer* **2005**, *46*, 4743–4752.
(28) Einstein, A. *Ann. Phys. (Leipzig)* **1906**, *19*, 289.
(29) Smallwood, H. J. *J. Appl. Phys.* **1944**, *15*, 758.
(30) Guth, E.; Gold, O. *Phys. Rev.* **1938**, *53*, 322.
(31) Batchelor, G. K. *An introduction to fluid dynamics*; Cambridge University Press: Cambridge, U.K., 1967.
(32) Cosgrove, T.; Roberts, C.; Choi, Y.; Schmidt, R. G.; Gordon, G. V.; Goodwind, A. J.; Kretschmer, A. *Langmuir* **2002**, *18*, 10075–10079.
(33) Kopesky, E. T.; Haddad, T. S.; Cohen, R. E.; McKinley, G. H. *Macromolecules* **2004**, *37*, 8992.
(34) Chambon, F.; Winter, H. H. *J. Rheol.* **1987**, *31*, 683.
(35) Winter, H. H.; Chambon, F. *J. Rheol.* **1986**, *30*, 367.
(36) Izuka, A.; Winter, H. H.; Hashimoto, T. *Macromolecules* **1992**, *25*, 2422–2428.
(37) Durand, D.; Delsanti, M.; Adam, M.; Luck, J. M. *Europhys. Lett.* **1987**, *3*, 97.
(38) Muthukumar, M. *Macromolecules* **1989**, *22*, 4656.
(39) Cassagnau, P. *Polymer* **2008**, *49*, 2183–2196.
(40) Chambon, F.; Petrovic, Z. S.; MacKnight, W. J.; Winter, H. H. *Macromolecules* **1986**, *19*, 2146–2149.
(41) Ding, Y.-X.; Weber, W. P. *Macromolecules* **1988**, *21*, 532–535.
(42) van Krevelen, D. W. *Properties of polymers*; Elsevier Science B. V.: Amsterdam, 1990.
(43) Price, G. J.; Shillcock, I. M. *J. Chromatogr. A* **2002**, *964*, 199–204.
(44) Barton, A. F. M. *CRC handbook of solubility parameters and other cohesion parameters*, 2nd ed.; CRC Press: Boca Raton, FL, 1991.
(45) Gordon, G. V.; Schmidt, R. G.; Quintero, M.; Benton, N. J.; Cosgrove, T.; Krukonis, V. J.; Williams, K.; Wetmore, P. M. *Macromolecules* **2010**, *43*, 10132–10142.
(46) Nakajima, N.; Varkey, J. P. *J. Appl. Polym. Sci.* **1998**, *69*, 1727.
(47) Ganesan, V.; Pyramitsyn, V.; Surve, M.; Narayanan, B. *J. Chem. Phys.* **2006**, *124*, 221102.
(48) Wang, M.; Hill, R. J. *Soft Matter* **2009**, *5*, 3940.
(49) Smith, G. D.; Bedrov, D.; Li, L.; Byutner, O. *J. Chem. Phys.* **2002**, *117*, 9478–9489.
(50) Termonia, Y. *Polymer* **2009**, *50*, 1062–1066.
(51) Starr, F. W.; Schroder, T. B.; Glotzer, S. C. *Phys. Rev. E* **2001**, *64*, 021802.
(52) Brown, D.; Mélé, P.; Marceau, S.; Albérola, D. *Macromolecules* **2003**, *36*, 1395–1406.
(53) Brown, D.; Marcadon, V.; Mélé, P.; Albérola, D. *Macromolecules* **2008**, *41*, 1499–1511.
(54) Roberts, C.; Cosgrove, T.; Schmidt, R.; Gordon, G. V. *Macromolecules* **2001**, *43*, 538–543.